High pH and Temperature Tolerant Molecular Mimics of Carbonic Anhydrase Towards Long-Term Carbonate Production in Enzymatic Construction Material

Rebecca J. Gilchrist,§ Peter G. Oni,§ Nima Rahbar,¶ Suzanne F. Scarlata,§* Ronald L. Grimm§*

§ Department of Chemistry & Biochemistry, Worcester Polytechnic Institute, Worcester, MA USA. ¶ Department of Civil Engineering, Worcester Polytechnic Institute, Worcester, MA USA.

* Address correspondence to grimm@wpi.edu, sfscarlata@wpi.edu

Keywords

Sustainable built environment

Catalysis

Green materials

Synopsis

The catalytic conversion of carbon dioxide into carbonate via molecules or enzymes is critical for clean air, minimizing global warming, and creating a sustainable built environment.

Abstract

We recently applied carbonic anhydrase (CA) for the rapid catalytic conversion of carbon dioxide to enable the self-healing properties of concrete and in the development of a carbon-negative concrete replacement named Enzymatic Construction Material (ECM). Here, we explore the stability and carbonate generation ability of model molecular mimics of carbonic anhydrase under high pH and elevated temperatures relevant to long-term durability in cementitious and concrete-like materials. Molecular mimics include Zn²⁺-based organometallic complexes with an aromatic ligand *tris*(2-pyridylmethyl)amine, TPA, and with an aliphatic ligand cyclen, 1,4,7,10-tetraazacyclododecane. The Zn(TPA) and Zn(cyclen) complexes are stable in aqueous environments at standard pressures ranging from neutral to pH 13 and temperatures up to 120 °C, where CA is inactive. Under the temperature and pH conditions studied, organometallic degradation pathways do not involve the decomposition of either organic ligand, but rather dissociation of the complex that is reversible upon neutralization in the case of Zn(TPA). Zn(cyclen) is stable at high temperatures at pH 12 and above, resembling cementitious conditions for over 365 days with no signs of degradation. Separately, alkaline calcium-containing solutions with either 25 nM CA or 5 mM Zn(cyclen) catalyst demonstrated accelerated pH decreases compared to catalyst-free controls upon sparging with carbon dioxide because of the conversion of CO₂ and H₂O to HCO₃⁻ and H⁺. Notably, the inclusion of sub-molar concentrations of detergents, such as sodium dodecyl sulfate, in carbonate production reactions demonstrated no change in the reactivity of control solutions or those with the Zn(cyclen) catalyst, but severely attenuated the conversion in CA-containing solutions concomitant with CA denaturation and loss of enzymatic activity.

1. Introduction

Concrete is a ubiquitous, low-cost construction material, with cement being the second most used substance in the world, only behind water.¹⁻² However, from production to transport, the concrete industry is a significant source of anthropogenic CO₂ and is responsible for approximately 8% of global emissions.³ Additionally, concrete is inherently brittle and prone to cracks and fractures, and repair involves additional financial, environmental, and labor costs. We recently reported that the biological enzyme carbonic anhydrase (CA) can be used to repair cracks and fractures in concrete. Additionally, CA enables the self-healing capability of concrete owing to the limited lifetime of the enzyme (i.e., ~2 weeks).⁴ CA, like all biological enzymes, has a short lifetime that is greatly reduced by the harsh environment of concrete, whose high curing temperature and highly basic nature will destabilize many molecules.

Developing a long-lived CA mimic that allows concrete self-healing for years or decades would decrease the waste and greenhouse gases associated with the replacement of concrete structures.

Another possible solution to the environmental costs associated with concrete is a less brittle and recyclable replacement. We recently developed an enzymatic construction material (ECM) that efficiently sequesters carbon and now has a strength approaching that of concrete.⁴⁶ ECM uses CA to catalyze the conversion of gas-phase atmospheric CO₂ to carbonate, CO₃²⁻, for the formation of calcium carbonate akin to non-hydraulic cement.⁴ The embedded CA in ECM allows the material to self-heal over 6 cycles.⁵⁻⁶ However, similar to concrete, this self-healing ability is limited by the short lifetime of CA.

The innate biological activity of carbonic anhydrase has been exploited for cementitious applications. CA, one of the fastest known enzymes, critically enables carbon dioxide transport out of the body via the reversible conversion of carbon dioxide to carbonate with catalytic rates of $\sim 10^6 \, \mathrm{M}^{-1} \mathrm{s}^{-1}$. However, CA is not stable for long

periods under cement-like conditions of high alkalinity and increased temperatures. ¹⁰⁻¹² Almost all variants of CA lose activity at 60 °C and in an environment of pH 9.5. ¹³⁻¹⁴ Ideally, CA operates at conditions below 40 °C and a pH of 7.5, ¹³ and the free enzyme loses its activity in minutes when in an alkaline solution. ¹⁵ Directed evolution and mutagenesis efforts have significantly improved the thermal stability of carbonic anhydrase, ¹⁶ but its pH stability remains limited. Beyond mutagenesis studies of carbonic anhydrase itself, research must also consider other approaches for including CA or CA-like structures for permanent incorporation into building materials with multidecadal lifespans.

Among non-enzymatic alternatives to carbonic anhydrase, organometallic compounds have received particular attention. Carbonic anhydrase was first identified nearly a century ago, 17 and over the last forty years, researchers have explored molecular mimics of CA both to elucidate its mechanism of reaction and to attempt to reproduce its high efficiency.^{8, 17-26} Relatedly, increasing demand for efficient CO₂ sequestration has driven research into CA mimics as a catalyst for carbon dioxide hydration and capture.²⁷⁻²⁹ Among organometallic molecular mimics of CA, complexes frequently incorporate tridentate aromatic pyridyl-based structures ligated to Zn²⁺ that reproduce the N₃ chelating effect from CA's three adjacent histidine residues of CA to yield species such as Zn²⁺-tris(2-pyridylmethyl)amine, Zn(TPA), as shown in Figure 1A. Previous studies determined that Zn(TPA) has a pH-dependent rate constant of ~650 M⁻ ¹s⁻¹ for carbon dioxide hydration.³⁰ Among aliphatic organometallic molecular mimics of CA, many complexes include azacyclic molecules that chelate the zinc atom within their structure. Zn²⁺ complexed to 1,4,7,10-tetraazacyclododecane, Zn(cyclen) (Figure 1B), is currently the most proficient aliphatic organometallic molecular mimic of CA at present time. 19, 21, 24-25, 31-32 Zn(cyclen) has N₄ chelating effects due to the cyclen structure and provides a high affinity for CO₂ hydration, with a pH-dependent rate constant of approximately 3300 M⁻¹s⁻¹.²⁵ Notably, Zn(cyclen) has been monitored in a slightly

alkaline environment towards industrial carbon dioxide capture and showed increased activity with increasing pH and temperature, ²⁷ but most research into CA molecular mimics focuses on biochemistry applications. With a nearly neutral pH, physiological conditions significantly depart from the highly alkaline pH environments in concrete that can reach as high as 13 during the hydration of calcium oxide and are thought to remain very high throughout the material's lifetime. Concrete maintains its strength and longevity in part because of its high alkalinity, where damage occurs, including rebar corrosion, when the pH is lowered. Furthermore, carbonate production demonstrates pH-dependence, so it is necessary to determine the stability and longevity of molecular mimics in extreme alkaline conditions as a long-term alternative for self-healing construction materials. Thus, it is necessary to understand how these organometallic molecular mimics behave at high pH and elevated temperatures to simulate the long lifetimes necessary for incorporation into cementitious materials. Such studies motivate the present investigation.

$$CO_2 + H_2O \xrightarrow{Catalyst} H^+ + HCO_3^-$$

$$Ca^{2+} + HCO_3^- \longrightarrow CaCO_3 + H^+$$

$$OH_2 \longrightarrow N \longrightarrow CaCO_3 + H^+$$

$$N \longrightarrow C$$

Figure 1. The conversion of CO_2 and H_2O to CO_3^{2-} utilizes a catalyst in biological and biomimetic environments. Canonical examples of molecular mimics of the biological catalyst carbonic anhydrase include (**A**) an aromatic ligand containing Zn^{2+} -(tris(2- pyridylmethyl)amine), Zn(TPA), and (**B**) the aliphatic-ligand-based Zn^{2+} -1,4,7,10-tetraazacyclododecane, Zn(cyclen), both of which contain ligated water in aqueous environments.

In this study, we investigated two molecular mimics of carbonic anhydrase as catalysts for ECM with high longevity and alkaline pH tolerance. The experiments

included stability studies in which aqueous-phase Zn(TPA) and Zn(cyclen) were subjected to periods of elevated temperatures and highly alkaline pH, which complemented other literature studies at somewhat more modest pH conditions.³⁵ NMR spectroscopy established the stability of each organometallic complex, the potential modes of degradation, and reformation pathways as a function of pH, temperature, and time. Beyond the catalyst stability, we further quantified carbonate production by introducing CO₂ into highly alkaline solutions relevant to cementitious conditions by observing pH changes over time, which allowed us to quantify carbonate production. Because of the higher rate constant for Zn(cyclen) vs. Zn(TPA), time studies of carbonate production have utilized only Zn(cyclen) as an alternative catalyst to carbonic anhydrase for calcium carbonate production with carbon sequestration. Carbonate production experiments alternatively utilized pH buffers, including Tris and CAPS, and buffer-free conditions. Finally, to establish the comparative effects of enzyme denaturants, some carbonate production experiments included small quantities of sodium dodecyl sulfate (SDS), an anionic surfactant that denatures proteins such as carbonic anhydrase. 36-39 Methods exist to decrease the rate of denaturing, 36 however, these were not explored in this work. We compared the results of the carbonate production experiments to literature CO2 sequestration results from alkaline solutions and discussed the viability of molecular mimics of CA for long-term incorporation into concrete and cementitious construction materials.

2. Experimental Section

2.1. Materials and Chemicals

Reagents were utilized without additional purification unless otherwise noted, including zinc perchlorate hexahydrate (Zn(ClO₄)₂·6H₂O, reagent grade, Thermo Scientific), zinc nitrate hexahydrate (Zn(NO₃)₂·6H₂O, 98%, extra pure, Acros Organics), 1,4,7,10-tetraazacyclododecane (cyclen, >97.0%, TCI), and *tris*(2-pyridylmethyl)amine,

(TPA, 98%, Combi-Blocks). The organic solvents used for synthesis and workup included acetone (99.5%, Thermo Scientific), ethanol (200% proof, ACS/USP grade, Pharmaco by Greenfield Global), and diethyl ether (99% min. stabilized with BHT; Alfa Aesar). The NMR solvents included deuterated chloroform (D, 99.8%, Cambridge Isotope Laboratories) and deuterium oxide (D, 99%, Cambridge Isotope Laboratories).

Chemicals employed in the calcium carbonate production include water from an in-house deionization system, 2-amino-2-(hydroxymethyl)propane-1,3-diol ("Tris" buffer, ≥99.8%, Fisher Scientific), *N*-cyclohexyl-3-aminopropanesulfonic acid, ("CAPS" buffer, 99%, Alfa Aesar), calcium formate (98%, Alfa Aesar, recrystallized in water), sodium hydroxide (98.5%, pellets, Acros Organics) and sodium dodecyl sulfate ("SDS", ≥98.5%, Sigma Aldrich). pXRD analysis was used to compare the precipitates formed during the carbonate production experiment against commercial calcium carbonate (98%, Alfa Aesar).

2.2. Synthesis of molecular complexes

Zn²⁺-(*tris*(2-pyridylmethyl)amine), Zn(TPA). Zn(TPA) syntheses followed previous procedures,³⁰ with a modification of using acetone rather than ethanol as the solvent, based on higher yields. Equimolar amounts of TPA (4.4 mmol, 1.2779 g) and zinc nitrate hexahydrate (4.4 mmol, 1.3433 g) were added to a Schlenk vial under an argon ambient. Separately, argon bubbling degassed 100 mL of acetone for 10–15 min directly preceding the syringe transfer of 66 mL to the solids with slow stirring. As the solids began to dissolve, the solution turned a burnt orange color and was left to stir overnight under an argon atmosphere. The following day, the solution had a sandy color with a noticeable precipitate. Following rotary evaporation to remove acetone, two rinsing cycles in diethyl ether yielded the final product, which was confirmed by ¹H and ¹³C NMR. (Yield: 93%)

Zn²⁺-(1,4,7,10-tetraazacyclododecane), Zn(cyclen). Based on literature procedures,²⁵ 10 mL acetone was added under an argon ambient to equimolar amounts of zinc perchlorate hexahydrate (0.87 mmol, 325 mg) and cyclen (0.87 mmol, 150 mg) with slow stirring. The reaction proceeded at 60 °C for 90 min. Rotary evaporation yielded a white solid, which was washed with ethanol and confirmed by ¹H and ¹³C NMR. (Yield: 78%)

2.3. Stability studies at elevated pH and temperatures

High-pH and elevated-temperature stability studies have utilized Zn(TPA) and Zn(cyclen) in aqueous environments. Stock solutions of aqueous sodium hydroxide at pH 9–14 were prepared directly prior to use to minimize the buffering effects of atmospheric carbon dioxide capture.

For pH stability experiments at ambient temperature, ~0.1 M of either Zn(TPA) or Zn(cyclen) was dissolved in 1 mL of NaOH_(aq) solution and covered. For all the Zn(TPA) samples, neutralization by dropwise addition of HCl_(aq) directly preceded NMR quantification following the reaction period. As neutralization can change the protonation state of the secondary amine in cyclen, NMR quantification of Zn(cyclen) considered both HCl_(aq)-neutralized and non-neutralized, highly alkaline samples. For HCl_(aq)-neutralized samples, rotary evaporation preceded dissolution in CDCl₃ for Zn(TPA) and D₂O for Zn(cyclen), whereas non-neutralized Zn(cyclen) samples were diluted in D₂O. 1H and 13C NMR analyses established changes in the structure of the Zn complex as a function of alkaline exposure. In instances of no demonstrable changes in the NMR spectra relative to each fresh Zn complex, the experiments were repeated with fresh reagents and longer time intervals until new spectral features ascribed to decomposition products appeared.

Thermal stability experiments on solutions of ~0.1 M of either Zn complex proceeded similarly to pH stability experiments. Rotary evaporation, dissolution in CDCl₃, and ¹H and ¹³C NMR spectroscopy were performed at each reaction time. As with the pH experiments, when NMR spectra demonstrated no decomposition-ascribable features, the experiments were repeated at that temperature for longer times. Following experiments that independently established pH stability at ambient temperature and thermal stability at near-neutral pH, we investigated the stability of both Zn(TPA) and Zn(cyclen) under simultaneously elevated temperatures and alkaline pH. As mentioned above, when ¹H NMR spectra demonstrated no change relative to each respective Zn complex, subsequent experiments with fresh reagents utilized a higher pH and increased temperature.

2.4. Monitoring Rate of Calcium Carbonate Formation Experiments

We contrasted the rate of carbonate formation in alkaline solutions with no added catalyst, with the molecular mimic Zn(cyclen) catalyst, or with the biological carbonic anhydrase catalyst. We further varied the presence of pH buffer, including CAPS, TRIS, and buffer-free conditions. Experiments quantified the time evolution of pH as a proxy for carbonate production, considering the reaction shown in Figure 1, where protons are a byproduct of the addition of carbon dioxide to water. We utilized carbonic anhydrase concentrations comparable to those utilized in producing the enzymatic construction material ECM.⁴ We did not consider Zn(TPA) in the carbonate-producing pH vs time experiments for its established slower second-order rate constant for carbonate production as compared to Zn(cyclen).^{27,30}

The catalysts were prepared individually for each experiment. A 100 μ M stock solution of carbonic anhydrase (3.08 mg in 1 mL water) was partitioned into 10 μ L aliquots that were kept frozen until use. Dilution into the 40 mL experimental volume

described below yielded a 25 nM concentration of active Zn²⁺ catalytic sites in the carbonic anhydrase during a carbonate-production experiment. Separately, experiments that included Zn(cyclen) utilized 1 mL of a 0.2 M aqueous solution that was degassed by active N₂ bubbling during preparation and throughout its addition to the experimental solution below. Diluted into the 40 mL experimental volume below yields a 5 mM concentration of active Zn²⁺ catalytic sites in the Zn(cyclen) during the carbonate-production experiments.

Calcium solutions were prepared as described in our previous work on CAbased enzymatic construction materials,4 with particular procedures designed to minimize any contribution from pre-dissolved carbon dioxide. The deionized water was initially degassed with N2 for ten minutes with stirring and continuous pH monitoring to establish a change from an initial value of ~5 to a final value of 7. For solutions that included pH buffers, 40 mL water portions sequentially received either 0.446 g (0.1 M) CAPS buffer or 0.244 g (0.1 M) Tris buffer followed by two minutes of nitrogen degassing, and 2.61 g (1.0 M) calcium formate with stirring. For pH-buffer-free solutions, 40 mL water portions sequentially received two minutes of nitrogen degassing, and 2.61 g (1.0 M) calcium formate with stirring. Each solution was further degassed with N2 while stirring for six minutes to ensure that the calcium formate was dissolved in an oxygen-and-CO₂ depleted solution. Upon complete dissolution of the calcium, sequential addition of one pellet of sodium hydroxide (approximately 0.1 g), six additional minutes of nitrogen degassing with stirring, and dropwise addition of a pH 13.5 NaOH_(aq) stock solution yielded a calcium-containing solution with a pH of 11.7. Solutions with pH = 11.7 solutions represent the catalyst-free "No Zn" mixtures considered below. Catalyst-containing mixtures alternatively involved the addition of either a thawed 10 µL 100 µM carbonic anhydrase solution or 1 mL of degassed 0.2 M Zn(cyclen)(aq).

To monitor carbonate production via the time evolution of pH, the nitrogen purging rate was reduced to 175 sccm using a commercial mass flow controller (Aera FC-770AC). Addition of 2.45 sccm of CO₂ (Aera FC-7700CU) to the nitrogen flow initiated each carbonate production experiment. The output from a high-impedance operational amplifier (Gravity analog pH sensor, Atlas Scientific, Long Island City, NY) was digitized (National Instruments USB-6009, Austin, TX, USA) and recorded in LabVIEW for storage and interpretation. Prior to each experiment, the pH sensor underwent two-point calibration at pH 7 and 10 using commercial calibration solutions (Myron L Company, Carlsbad, CA).

To establish the effect of protein denaturation on the behavior of CA beyond its normal structural lifespan, we added SDS to the carbonate production experiments with CA as the catalyst, Zn(cyclen) as the catalyst, and no catalyst as the control. For SDS-containing experiments, 1 mL of an aqueous stock solution of 5 mM SDS (1.41 mg) was further diluted to 50 μ M. For carbonate production experiments with Zn(cyclen) as the catalyst, we added 10 μ L of 5 mM SDS(aq) to 1 mL of 0.2 M Zn(cyclen) prior to its addition into the degassed calcium solution. For carbonate production experiments with carbonic anhydrase, 10 μ L of 50 μ M SDS (aq) was added to a 10 μ L aliquot of 100 μ M carbonic anhydrase prior to freezing, as described above. For the catalyst-free control experiment, 10 μ L of 5 mM SDS (aq) was added to the degassed calcium-containing solution directly preceding the experiments.

Further investigation into catalyst degradation examined the catalysts left in a 50 °C bath for two weeks. These experiments followed the same procedures outlined above, except that the catalyst stock solution remained in a 50 °C bath until it was ready for degassing steps, following the procedures described above.

Following the carbonate production experiments, XRD experiments established that the solid product was CaCO₃. A benchtop Rigaku MiniFlex powder X-ray diffractometer with Cu K α radiation was used to collect X-ray diffraction (XRD) traces

in the range of 3°–90° (2θ). The samples were tape-adhered to a stage for analysis under ambient air, following drying. Dried, solid mass quantified the total yield accounting for the high relative solubility of CaCO₃ in aqueous formic acid solution.³⁹⁻⁴⁰ Separately, we dissolved 2.002 g CaCO₃ in 20 mL of 2 mM aqueous formic acid, yielding a total mass of dried, non-dissolved CaCO₃ of 0.314 g (16% yield). We used this resulting mass to represent a 100% yield of dried CaCO₃ in the carbonate production experiments.

3. Results

3.1. High pH and Elevated Temperature Stability Studies

Figure 2 presents representative ¹H NMR spectra that reveal the stability, decomposition, and reformation of Zn(TPA) at elevated pH and temperatures. Figures S1–4 in the Supporting Information section present the corresponding ¹³C NMR spectra for each respective ¹H NMR trace in Figure 2A–D. Each trace in Figure 2 demonstrates a feature at δ = 7.26 ppm due to CHCl₃ contamination in the CDCl₃ solvent, as well as spinning sidebands at ±0.21 ppm in frame D that we do not consider further. The ¹H NMR spectrum of TPA in Figure 2A demonstrates features consistent with previous reports, including six benzylic hydrogens at δ = 3.93 ppm, as well as a three-proton doublet at 7.58 ppm, a three-proton triplet at 7.65 ppm, a three-proton triplet at 7.15 ppm, and a three-proton doublet at 8.54 ppm for the aryl hydrogens at positions 3–6 around the pyridine ring.²⁷ Following complexation with Zn²⁺, the ¹H NMR spectrum of Zn(TPA) in Figure 2B demonstrates a downfield shift for each feature that is consistent with other reports.³⁰

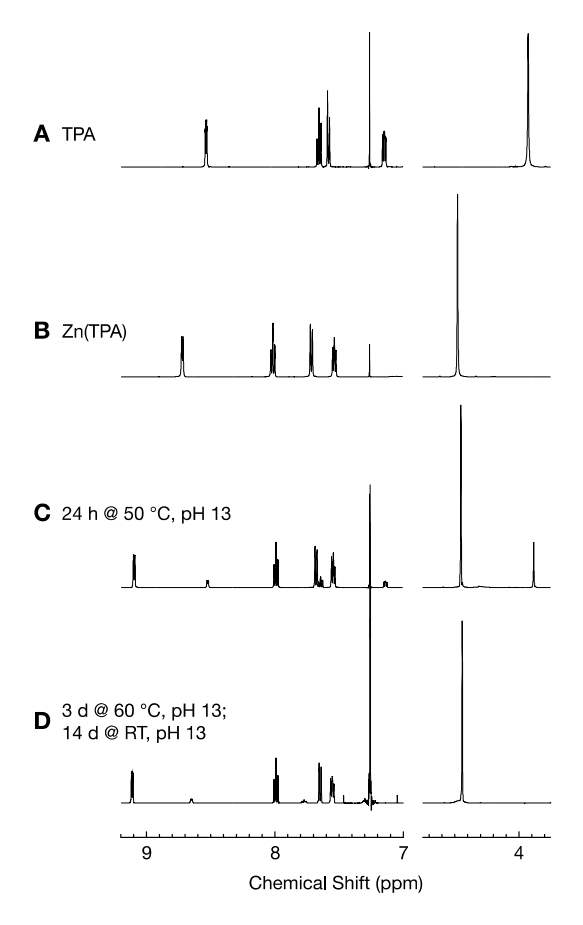


Figure 2. Features in the 1 H NMR spectrum of TPA (**A**) demonstrated downfield shifts when ligated to Zn^{2+} in Zn(TPA) (**B**). After 24 h in an aqueous, pH 13 environment at 50 °C, which mimics the extremes of cementitious environments, the 1 H NMR in (**C**) demonstrates features due to both complexed Zn(TPA) and free TPA. Interestingly, the dissociated species from (**C**) demonstrated partial reassociation into Zn(TPA) in a dilute solution when left at room temperature in an alkaline solution, as shown in (**D**). Deleterious CHCl₃ yields the feature at 7.26 ppm with spinning sidebands further observed in frame (**D**).

Elevated temperatures and extremely alkaline pH conditions affect the changes in Zn(TPA). We chose pH 13 solutions to mimic the extreme of the alkaline environment that exists in cementitious materials.³³ In our hands, we observed no notable deviation from the spectrum in Figure 2B for Zn(TPA) in pH 13 solutions at room temperature for up to 32 days. However, Figure 2C demonstrates additional NMR-observable features when heated to 50 °C at pH 13 for 24 h. Figure 2C demonstrates both downfield-shifted clusters characteristic of Zn(TPA) from Figure 2B,

as well as clusters in the original locations of the nascent TPA, as shown in Figure 2A. While the *ortho* protons relative to the pyridine nitrogen shift from δ = 8.54 ppm in TPA to 8.73 ppm when ligating Zn²⁺ in Zn(TPA), these protons demonstrate a further downfield shift to 9.1 ppm in the pH 13 spectrum in Figure 2C. Taken together, we attribute the observable Zn(TPA) and free TPA in Figure 2C to the small amount of dissociation of the Zn²⁺-TPA complex at this elevated temperature and alkaline pH. Importantly, Figure 2C reveals no additional features that would otherwise indicate decomposition of the TPA ligand. Frame D in Figure 2 presents a spectrum of Zn(TPA) from a pH 13 solution that was sequentially heated at 60 °C for three days to initiate the dissociation of the Zn(TPA) complex, followed by room temperature for 14 days in the same pH 13 environment. In contrast to frame C with free-TPA-ascribable peaks, Figure 2D shows only trace amounts of free TPA with predominantly Zn(TPA) features with no additional features beyond CHCl₃ contamination. We attribute the results in Figure 2D to indicate that any dissociation of the Zn(TPA) ligand complex at pH 13 and 60 °C yields reassociation when returned to room temperature, even at elevated pH. Reassociation and reformation of the Zn(TPA) complex at alkaline pH and room temperature is broadly consistent with picomolar binding affinities between Zn²⁺ and TPA.41

Figure 3 presents the representative 1 H NMR spectra for Zn(cyclen) and its behavior at elevated pH and temperature. Figures S5–9 in the Supporting Information section present the corresponding 13 C NMR spectra for each respective 1 H NMR trace in Figure 3A–E. From Figure 3A, the cyclen starting material demonstrates a δ = 2.65 ppm singlet whose symmetry is broken upon Zn²⁺ ligation yielding the doublet of multiplets at 2.84 ppm and 2.97 ppm in Figure 3B.²⁷ The spectra in frames A and B are broadly consistent with other literature reports of Zn(cyclen) due to the uneven ligation of Zn²⁺ by the nitrogen atoms around the cyclen ring.^{25,27} Further exposure to pH 13 at 96 °C for 6 days yields spectra as in Figure 3C with direct dilution in D₂O and no

neutralization that presents irresolvable multiplet splitting in our 500 MHz instrument. An additional feature at δ = 3.40 ppm in Figure 3C is consistent with cyclen N–H protons at elevated pH as observed elsewhere.³⁵ Beyond the comparatively short timescale in frame C, frame D in Figure 3 presents the results for Zn(cyclen), which was maintained in a capped vessel at pH 13.5 at 120 °C for more than 365 days (1 year), then neutralized directly preceding dilution in D₂O and NMR. Notably, the spectrum in Figure 3D matches that in frame B, indicating high longevity for the Zn(cyclen) complex under high thermal and aqueous alkaline conditions that are in excess of the cement curing conditions. Lastly, Figure 3E presents the NMR spectra for Zn(cyclen) after 40 days at – 5 °C, indicating stability to cold temperatures in addition to the higher temperatures above.

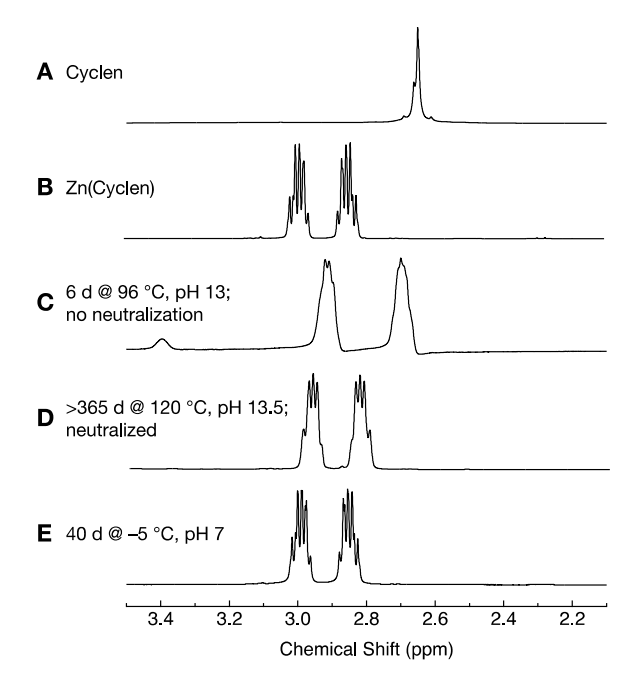


Figure 3. ¹H NMR establishes the Zn(cyclen) stability relevant to cementitious environments relative to (A) cyclen, starting material, and (B) a freshly prepared Zn(cyclen) complex. Zn(cyclen) demonstrates stability and longevity at high temperatures and alkaline conditions following (C) six days at pH 13 and 96 °C with no neutralization prior to NMR, and (D) more than 365 days at 120 °C and pH 13.5, and neutralization directly preceding NMR. Maintaining – 5 °C for 40 days, as in (E), further demonstrates the stability of the Zn(cyclen) complex.

3.2. Calcium Carbonate Formation Studies

Carbonate-formation-vs-time experiments from high-pH solutions enable comparisons of the catalytic behavior between biological carbonic anhydrase, its molecular mimics, and catalyst-free controls relevant to cementitious conditions. Monitoring pH versus time provides a real-time proxy for reactivity, in which faster transitions from alkaline to neutral pH correspond to faster carbonate formation. As previous biologically motivated studies found bimolecular rate constants to be almost five times higher for Zn(cyclen) than for Zn (TPA) near neutral pH, 27 we only compared Zn(cyclen) with CA in time studies of carbonate formation from a highly alkaline pH relevant to construction materials.

The final product of the carbonate formation experiments presented in this section is solid calcium carbonate. In each individual experiment, the solutions quickly turned cloudy upon the introduction of CO₂ into the sparged stream. As shown in Figure S10 in the Supporting Information section, the XRD patterns of the dried solids match well with both literature traces and scans of commercially available CaCO₃ with no features ascribable to other species within the detection limits. Following filtration and drying at 120 °C overnight, the total mass of solid calcium carbonate was ~16% of the stoichiometric yield. This low yield is consistent with the high solubility of calcium carbonate in formic acid,^{40, 42} where we consider formate from the calcium reagent and the production of protons throughout these experiments by the reactions in eq 1.

Figure 4 presents representative carbonate-formation-time experiments with varying pH buffers and no added catalyst. Thus, the pH changes associated with carbon dioxide uptake are driven solely by the alkalinity of the starting solution. In Figure 4, the fine dotted line corresponds to the pH-vs-time trace for a buffer-free solution, the dashed line corresponds to the inclusion of 0.1 M Tris, and the solid line

corresponds to the addition of 0.1 M CAPS. Figure 4 further includes the point at which the traces for the buffered solutions pass the pKa values of CAPS and the 8.1 p K_a of Tris at 25 °C. The pH vs. time traces of the buffer-containing solutions demonstrate a slower transition towards neutral pH relative to the buffer-free solution, which is consistent with the increased buffering capacity of CAPS and Tris towards carbonate production. Interestingly, the pH-vs-time trace of the CAPS-buffered solution matches the literature traces for CO₂ absorption experiments that monitor pH vs. time for carbonate production in alkaline monoethanolamine (MEA)-containing solutions.⁴³ Notably, the p K_a of monoethanolamine (MEA) is 9.5, which is somewhat close to the p K_a of CAPS, which may in part support the similarity in their carbonate production behavior. The high p K_a of CAPS relative to the other compounds, its similarity to cement pH during hydration, and its capacity to buffer carbonate production motivates the use of CAPS for all ongoing catalysis studies below. Additionally, the presence of a buffer increased the CO₂ sorption capability of these solutions relative to that of an unbuffered solution.

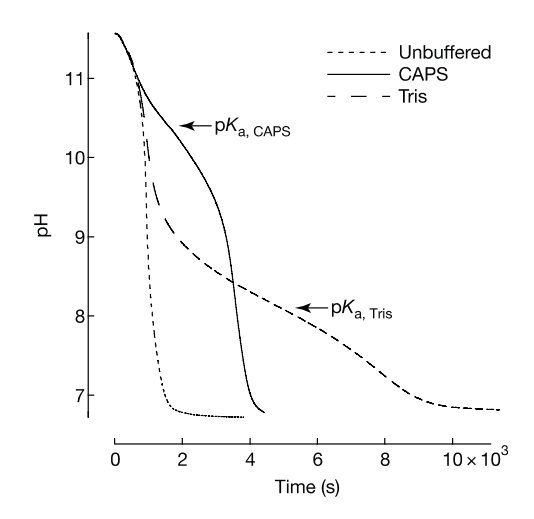


Figure 4. Evolution of pH versus time in alkaline solutions during CO₂ bubbling as a function of the solution buffer. The addition of alkaline buffers such as CAPS (solid) and Tris (dashed) yields a significant slowdown in pH neutralization, which is concomitant with an increased capacity for CO₂ absorption for buffered solutions relative to unbuffered solutions (dotted line). The shape of each pH vs. time graph was consistent with the acid dissociation constant of each buffer.

The addition of either Zn(cyclen) or carbonic anhydrase accelerates carbonate production relative to the catalyst-free control. Figure 5 presents representative pH–time traces for CO2 absorption and carbonate conversion in CAPS-buffered solutions with no added catalyst (black), 25 nM carbonic anhydrase (red), and 5 mM Zn(cyclen) (cyan). The black trace without added catalyst in Figure 5 reproduces the CAPS-buffered data in the solid line in Figure 4. Relative to the catalyst-free case, the addition of either the CA or the Zn(cyclen) catalyst yields a more rapid drop in pH in the high-pH regime between the initial pH > 11.5 and a pH of ~10. Importantly, the rate of pH change was similar for the CA catalyst trace and the Zn(cyclen) trace, despite the 2×10^5 higher concentration of Zn(cyclen). The relative difference in concentrations between CA and Zn(cyclen) implies that their rate constant differences are even greater than those found in near-neutral pH experiments elsewhere. In contrast to the high pH regime, the profiles of each trace in Figure 5 are largely similar to each other at modestly alkaline pH values between pH 9 and 7, albeit with shifts in time based on the higher pH behavior.

The literature on monoethanolamine-buffered CO₂ absorption and carbonate conversion elucidates the processes involved in Zn-catalyzed studies in Figure 5. Researchers ascribe the overall shape of curves in monoethanolamine-buffered CO₂ absorption to an initial fast, exothermic, and catalyst-driven reaction under conditions of low CO₂ loading and highly alkaline pH followed by a slower reaction corresponding to the non-catalyzed hydration of CO₂.⁴³⁻⁴⁴ Further, carbon dioxide absorption rates decrease with increased CO₂ loading, which fits the spline-shaped curve corresponding to unbuffered carbonate conversion.⁴³ Monoethanolamine models capture the salient details in Figure 5, where the CA and Zn(cyclen) catalysts accelerate CO₂ absorption at high pH with little to no catalytic impact at only modestly alkaline pH values. Furthermore, the absence of a significant catalytic impact at pH values below 9 further

supports why the ~1 × 10^3 -fold difference in rate constants between CA and Zn(cyclen) at biological pH does not represent the 2 × 10^5 -fold higher concentration of Zn(cyclen) required to match its rate to CA at highly alkaline pH.

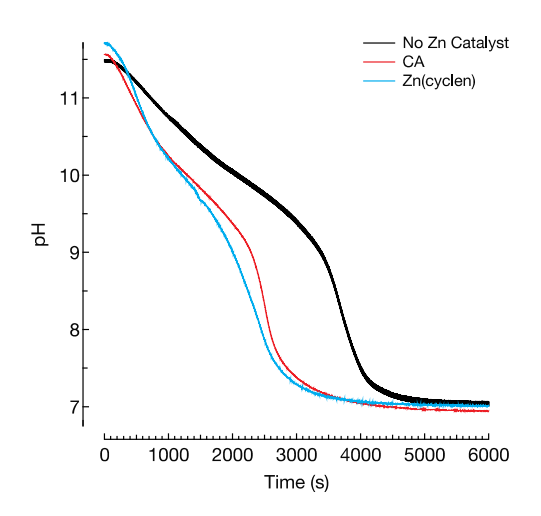


Figure 5. Relative to a representative Zn-catalyst-free control (black), the addition of CA (red) or Zn(cyclen) (cyan) accelerated carbonate production at highly alkaline pH values above 10 with little to no catalytic impact between pH 9 and 7.

Relevant to long-term self-healing and carbonate production in cementitious materials, it is critical to understand how molecular mimics of carbonic anhydrase behave under conditions that may degrade the performance of CA itself. Figure 6 shows the data from Figure 5 and includes pH vs. time traces for carbonate production experiments with an added enzyme denaturant, SDS. In the presence of $1.3~\mu M$ SDS, the dashed cyan line in Figure 6 for the 5 mM molecular Zn(cyclen) catalyst demonstrates a modest reduction in carbonate production relative to the non-SDS-spiked Zn(cyclen) catalyst (cyan line), but remains faster compared to the catalyst-free control. The dashed red line in Figure 6 indicates severely diminished carbonate production rates for carbonic anhydrate-containing solutions when spiked with 12.5 nM SDS relative to the catalyzed rate for the 25 nM CA catalysis in the solid red line and relative to the catalyst-free control. Importantly, the addition of SDS only appears to

change the rate of carbonate production and pH changes for pH values above 9, with little change in the overall shape due to SDS for carbonate production between pH 9 and 7. This SDS influence further supports the model established by the monoethanolamine studies considered above, in which the rates between the initial pH of 11.7 and pH 9 are most influenced by the catalysts. That SDS decreases the carbonate production rate for carbonic anhydrase is consistent with the established proteindenaturing behavior of SDS.⁴⁵ In contrast to CA, the addition of SDS only weakly affected the rate of carbonate formation and pH change for Zn(cyclen) solutions. The dashed blue line in Figure 6 for pH-vs-time carbonate formation for SDS-containing Zn(cyclen) is only modestly shifted to slower rates than non-SDS-containing Zn(cyclen) solutions. Thus, in contrast to CA which shows complete degradation of catalytic performance due to SDS, chemical degradation only modestly affects the catalytic nature of Zn(cyclen) towards carbonate production under cement-relevant conditions.

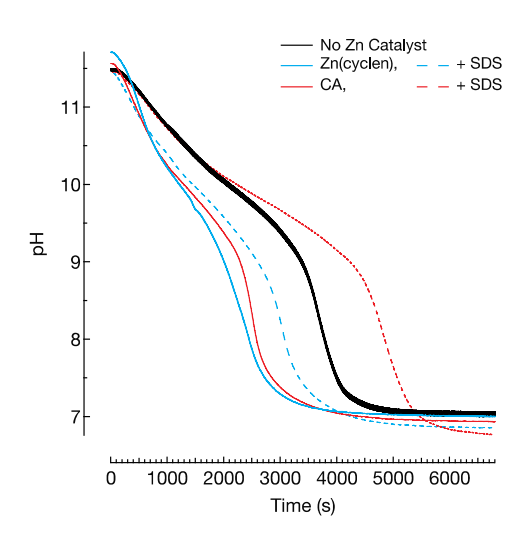


Figure 6. The addition of the denaturing surfactant SDS in frame C has little impact on the carbonate production rate for the Zn(cyclen)-containing solution (dashed blue line vs. solid blue line), while SDS decreased the carbonate production rate for a carbonic anhydrase-containing solution (dashed red line vs. solid red line).

To further confirm the potential degradation of carbonic anhydrase under cementitious conditions, we examined heat-treated CA and the impact of extended time in warm environments on catalytic activity. The pH-vs-time dashed line trace in Figure 7 utilized CA that had endured 50 °C for two weeks prior to utilization. As mentioned above, the black trace in Figure 7 represents a catalyst-free control, as shown in Figures 5 and 6. The near-uniformity in shape between the two traces in Figure 7 further supports the idea that CA is catalytically dead following a two-week exposure to 50 °C and provides no benefit for carbonate formation.

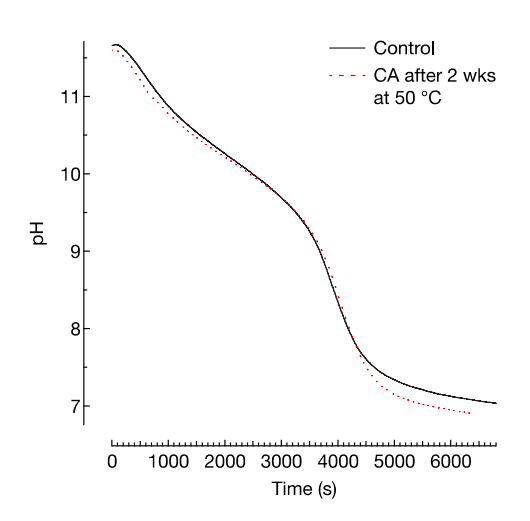


Figure 7. Utilization of CA that had been exposed to 50 °C for two weeks prior to use yielded pH-vs-time traces for carbonate formation (dotted red line) that resemble control experiments with no added catalyst (black line).

4. Discussion

Increased atmospheric carbon dioxide levels are a growing concern for society. With the constant need for new infrastructure and the huge toll of cement production on the environment, a low-cost and robust carbon-negative construction material is pivotal.

Both non-traditional cementitious materials and cement-based carbon capture materials must survive under extreme conditions for extended periods of time. Our recent use of carbonic anhydrase established the viability of an enzymatic approach both to produce novel construction materials and to heal defects in concrete.⁴⁻⁶

However, the short lifetime of carbonic anhydrase relative to the lifetime of cementitious materials and instability towards thermal or chemical denaturing has motivated the search for alternatives. When comprised of oxidatively and thermally stable pyridine groups and simple aliphatic amines, the present results demonstrate that many classic molecular mimics of the CA active site demonstrate high thermal and pH stability under typical curing conditions for cement.^{25, 27, 30, 32} However, one critical trade-off for the increased stability of the organometallic molecular mimics is a severely attenuated rate for carbonate formation relative to the evolutionarily optimized carbonic anhydrase enzyme. Previous studies near biological pH noted more than a three-order-of-magnitude difference in the second-order rate constants for CA relative to even the best molecular mimics. In the present study, carbonate production quantified by the pH vs. time experiments, as shown in Figure 5, utilized a 2 × 10⁵-fold higher concentration of the molecular mimic Zn(cyclen) to achieve rates comparable those to of carbonic anhydrase. CA achieves its high speed not only from its Zn²⁺ active site but also from the surrounding superstructure that not only orients water relative to carbon dioxide, but also includes a proton shuttle that minimizes the possibility of a back reaction between the proton and the newly formed bicarbonate.

Primary and secondary amines, such as monoethanolamine (MEA), are well-established routes for post-combustion CO₂ capture in industry. ^{27, 43-44, 46-52} Aqueous MEA solutions are predominantly used as a standard in carbon capture. Studies have reported the mechanism of CO₂ loading and the role of pH in MEA activity to convert CO₂ to product and showpH curves similar to those shown in this work. The studies outlined above follow similar kinetic pathways to this well-studied mechanism in alkaline solutions: an initial rapid decrease in pH due to the initial uptake of CO₂ in low-loading solutions, followed by a slower pH change due to the increased CO₂ loading, and the primary reaction being the direct hydration of carbon dioxide to form

carbonate. The CO₂-absorption capacity linearly as the CO₂ loading in the solution increased.

Based on the MEA literature, we divided our pH vs. time data into two regimes: the catalytic regime that occurs until the pH of the solution reaches pH = 9 and from pH = 9 to pH = 7, is considered the direct hydration regime. In the catalytic regime, from an initial alkaline pH of \sim 11.7 to a mildly alkaline pH of 9, the catalysts alter the shape of the curve, as seen in Figure 5. Without a catalyst (solid black), the catalytic regime exhibited a linear decline, whereas the addition of molecular or biological catalysts caused a drastic decline in reaction rate. Below pH = 9, all curves, both with and without the catalyst, display the same shape; this is because the main reaction becomes the direct hydration of CO₂, which does not rely on catalytic activity.

Kinetic studies of Zn(cyclen) were performed at a slightly alkaline pH. A previous study reported a sigmoidal relationship between the second-order rate constant and the alkalinity of the solution. The highest pH examined in this study was using the Ches buffer which yielded a pH = 9.11 and a rate constant of 3300 M⁻¹s⁻¹.²⁵ Based on previous kinetics studies of Zn(cyclen) and MEA literature, we believe the initial rates in the catalytic regime are driven by the low initial loading of carbon dioxide and the nucleophilicity of the zinc bound hydroxyl in alkaline conditions. As the pH decreased, the CO₂ loading in the solution increased and direct hydration became the predominant reaction at pH values below 9.

Our work prioritizes the catalytic regime and treats these studies as a race to pH = 9, which is particularly relevant to cementitious materials, as the hydration reaction proceeds at pH values in excess of 11. The addition of molecular and enzymatic catalysts drastically affected the time required to reach the direct hydration regime, as shown in Figure 5. However, the addition of SDS to CA resulted in a catalytic regime similar to that of the control. We attributed this to enzymatic catalyst death. When SDS was added to Zn(cyclen) solutions, a slight change in the rate was observed; however,

the shape of the catalytic regime was not impacted, meaning that the structure and activity of Zn(cyclen) remain unaffected by the addition of a chemical denaturant such as SDS.

Although carbonic anhydrase has an optimized structure to produce bicarbonate, it falls short as a long-term catalyst for carbon negative alternatives in the cement industry owing to its long-term instability in highly alkaline environments and reliance on the secondary structure. Molecular mimics, such as Zn(cyclen), require an increased concentration to produce rates comparable to those of the enzyme; however, they do not degrade under cementitious conditions and therefore have the potential to be an alternative to current methods for utilizing anthropogenic CO₂ to create a new construction material.

The presently quantified rate differences reinforce the exceptional catalytic performance of carbonic anhydrases relative to the best molecular alternatives.

Tradeoffs between stability and speed require further research to determine whether a sweet spot exists for molecular mimics that more closely reproduce CA's structure and speed of CA without sacrificing high pH or thermal stability. Considerations for the large-scale global deployment of such molecular catalysts would require synthetic techniques with brutally low cost compared to the synthesis of fine chemicals, while also not contributing to CO₂ release. Future views of molecular mimics that reproduce CA's pocket structure of CA and localization of hydrophobic/hydrophilic components would certainly benefit from technoeconomic insights into the cost/benefit tradeoff between catalytic rate increases and the scalable deployment of carbonate-producing catalysts for either non-traditional cementitious materials or cement-based carbon capture materials.

5. Conclusions and Future Work

Two Zn²⁺-based organometallic molecular mimics of carbonic anhydrase, Zn(TPA) and Zn(cyclen), demonstrate thermal and alkaline stability relevant for carbonate production in both non-traditional cementitious materials and cement-based carbon capture materials. Proton NMR experiments at alkaline pH and elevated temperature beyond that of typical cementitious environments demonstrates that the predominant mode of decomposition for Zn(TPA) and Zn(cyclen) is the reversible dissociation of the Zn²⁺ from its ligand where modest decreases in pH reforms the organometallic complex. The fact that each complex is stable beyond pH 12 and temperatures beyond 50 °C indicates that these complexes would survive cementitious environments and the particularly exothermic alkaline curing process.

Studies of carbonate formation have quantified pH changes from highly alkaline solutions to neutral pH as a function of time with and without a catalyst. The inclusion of carbonic anhydrase significantly increased the rate of carbonate formation and achieved a rate comparable to of that the Zn(cyclen) catalyst, which required a 2 × 10⁵-fold higher concentration relative to CA itself. Future studies may target modest, inexpensive changes to the organometallic complex that better capture the CA catalytic superstructure without degrading its high pH stability.

6. Author Information

Corresponding Authors:

Ronald L. Grimm – WPI Life Science and Bioengineering Center, Department of Chemistry and Biochemistry, Worcester Polytechnic Institute, 100 Institute Road, Worcester, Massachusetts 01609, United States; orcid.org/0000-0003-0407-937X; Email: grimm@wpi.edu

Suzanne F. Scarlata – WPI Life Science and Bioengineering Center, Department of Chemistry and Biochemistry, Worcester Polytechnic Institute, 100 Institute Road,

Worcester, Massachusetts 01609, United States; orcid.org/0000-0001-5652-7467; Email: sfscarlata@wpi.edu

Authors:

Rebecca J. Gilchrist – WPI Life Science and Bioengineering Center, Department of Chemistry and Biochemistry, Worcester Polytechnic Institute, 100 Institute Road, Worcester, Massachusetts 01609, United States; orcid.org/0009-0005-2218-6373

Peter G. Oni – WPI Life Science and Bioengineering Center, Department of Chemistry and Biochemistry, Worcester Polytechnic Institute, 100 Institute Road, Worcester, Massachusetts 01609, United States; orcid.org/0000-0001-5750-7476

Nima Rahbar –Department of Civil, Environmental and Architectural Engineering,
Worcester Polytechnic Institute, 100 Institute Road, Worcester, Massachusetts 01609,
United States; orcid.org/0000-0003-0159-0025

7. Acknowledgments

The authors acknowledge the financial support from the NSF CMMI–2223664.

8. References

- 1. Gagg, C. R., Cement and Concrete as an Engineering Material: An Historic Appraisal and Case Study Analysis. *Eng. Failure Anal.* **2014**, *40*, 114-140. https://doi.org/10.1016/j.engfailanal.2014.02.004
- 2. Andrew, R. M., Global CO₂ Emissions from Cement Production. *Earth Syst. Sci. Data* **2018**, *10*, 195-217. https://doi.org/10.5194/essd-10-195-2018
- 3. Joint Research, C.; Institute for, E.; Sustainability; Olivier, J.; Janssens-Maenhout, G.; Peters, J., *Trends in Global CO₂ Emissions: 2012 Report*, Publications Office, 2013. https://doi.org/10.2788/33777
- 4. Rosewitz, J. A.; Wang, S.; Scarlata, S. F.; Rahbar, N., An Enzymatic Self-Healing Cementitious Material. *Appl. Mater. Today.* **2021**, *23*. https://doi.org/10.1016/j.apmt.2021.101035
- 5. Wang, S.; Scarlata, S.; Rahbar, N., Curing and Self-Healing of Enzymatic Construction Materials Using Nanoparticles. *Cell Rep. Phys. Sci.* **2022**, *3*, 101039. https://doi.org/10.1016/j.xcrp.2022.101039
- 6. Wang, S.; Scarlata, S. F.; Rahbar, N., A Self-Healing Enzymatic Construction Material. *Matter* **2022**, *5*, 957-974. https://doi.org/10.1016/j.matt.2021.12.020
- 7. Khalifah, R. G., The Carbon Dioxide Hydration Activity of Carbonic Anhydrase: I. Stop-Flow Kinetic Studies on the Native Human Isoenzymes B and C. *J. Biol. Chem.* **1971**, *246*, 2561-2573. https://doi.org/10.1016/S0021-9258(18)62326-9
- 8. Steiner, H.; Jonsson, B.-H.; Lindskog, S., The Catalytic Mechanism of Carbonic Anhydrase. *Eur. J. Biochem.* **1975**, *59*, 253-259. https://doi.org/10.1111/j.1432-1033.1975.tb02449.x
- 9. Lindskog, S., Structure and Mechanism of Carbonic Anhydrase. *Pharmacol. Ther.* **1997**, *74*, 1-20. https://doi.org/10.1016/S0163-7258(96)00198-2
- Heveran, C. M.; Williams, S. L.; Qiu, J.; Artier, J.; Hubler, M. H.; Cook, S. M.; Cameron, J. C.; Srubar, W. V., Biomineralization and Successive Regeneration of Engineered Living Building Materials. *Matter* 2020, *2*, 481-494. https://doi.org/10.1016/j.matt.2019.11.016

- 11. Jonkers, H. M.; Thijssen, A.; Muyzer, G.; Copuroglu, O.; Schlangen, E., Application of Bacteria as Self-Healing Agent for the Development of Sustainable Concrete. *Ecol. Eng.* **2010**, *36*, 230-235. https://doi.org/10.1016/j.ecoleng.2008.12.036
- 12. Lavecchia, R.; Zugaro, M., Thermal Denaturation of Erythrocyte Carbonic Anhydrase. *FEBS Lett.* **1991**, *292*, 162-164. https://doi.org/10.1016/0014-5793(91)80858-Z
- 13. Demir, Y.; Demir, N.; Nadaroglu, H.; Bakan, E., Purification and Characterization of Carbonic Anhydrase from Bovine Erythrocyte Plasma Membrane. *Prep. Biochem. Biotechnol.* **2000**, *30*, 49-59. https://doi.org/10.1080/10826060008544944
- 14. Kanbar, B.; Ozdemir, E., Thermal Stability of Carbonic Anhydrase Immobilized Within Polyurethane Foam. *Biotechnol. Prog.* **2010**, *26*, 1474-1480. https://doi.org/10.1002/btpr.452
- 15. Molva, M.; Kilic, S.; Ozdemir, E., Effect of Carbonic Anhydrase on CaCO₃ Crystallization in Alkaline Solution. *Energy Fuels* **2016**, *30*, 10686-10695. https://doi.org/10.1021/acs.energyfuels.6b02475
- 16. Molina-Fernández, C.; Luis, P., Immobilization of Carbonic Anhydrase for CO₂ Capture and Its Industrial Implementation: A Review. *J. CO₂ Util.* **2021**, *47*, 101475. https://doi.org/10.1016/j.jcou.2021.101475
- 17. Smith, K. S.; Ferry, J. G., Prokaryotic Carbonic Anhydrases. *FEMS Microbiol. Rev.* **2000**, *24*, 335-366. https://doi.org/10.1111/j.1574-6976.2000.tb00546.x
- 18. Bergquist, C.; Fillebeen, T.; Morlok, M. M.; Parkin, G., Protonation and Reactivity Towards Carbon Dioxide of the Mononuclear Tetrahedral Zinc and Cobalt Hydroxide Complexes, [Tp^{But,Me}]ZnOH and [Tp^{But,Me}]CoOH: Comparison of the Reactivity of the Metal Hydroxide Function in Synthetic Analogues of Carbonic Anhydrase. *J. Am. Chem. Soc.* **2003**, *125*, 6189-6199. https://doi.org/10.1021/ja034711j
- 19. Brown, R. S., Trisimidazolylphosphine: M(II); Models for the Metal-Binding Site in Carbonic Anhydrase. *Inorg. Chim. Acta* **1983**, *79*, 64-65. https://doi.org/10.1016/S0020-1693(00)95091-6
- 20. Kato, M.; Ito, T., Facile CO₂ Uptake by Zinc (II)-Tetraazacycloalkane Complexes. 1. Syntheses, Characterizations, and Chemical Properties of (Monoalkyl carbonato)(tetraazacycloalkane) Zinc (II) Complexes. *Inorg. Chem.* **1985**, *24*, 504-508. https://doi.org/10.1021/ic00198a015

- 21. Looney, A.; Parkin, G., Molecular Structure of { η ³-HB(pz)₃}ZnNO₃: Comparison between Theory and Experiment in a Model Carbonic Anhydrase System. *Inorg. Chem.* **1994**, *33*, 1234-1237. https://doi.org/10.1021/ic00084a045
- 22. Palmer, D. A.; Van Eldik, R., The Chemistry of Metal Carbonato and Carbon Dioxide Complexes. *Chem. Rev. (Washington, DC, U. S.)* **1983**, *83*, 651-731. https://doi.org/10.1021/cr00058a004
- 23. Parkin, G., Synthetic Analogues Relevant to the Structure and Function of Zinc Enzymes. *Chem. Rev. (Washington, DC, U. S.)* **2004**, *104*, 699-768. https://doi.org/10.1021/cr0206263
- 24. Slebocka-Tilk, H.; Cocho, J. L.; Frackman, Z.; Brown, R. S., Carbonic Anhydrase Models. 5. Tris(4,5-di-*n*-propyl-2-imidazolyl)phosphine-Zinc²⁺ and bis(4,5-di-isopropyl-2-imidazolyl)-2-imidazolylphosphine-Zinc²⁺. Catalysts Facilitating Hydrogen Carbonate <-> Carbon Dioxide (HCO₃- <-> CO₂) Interconversion. *J. Am. Chem. Soc.* **1984**, *106*, 2421-2431. https://doi.org/10.1021/ja00320a032
- 25. Zhang, X.; van Eldik, R., A Functional Model for Carbonic Anhydrase: Thermodynamic and Kinetic Study of a Tetraazacyclododecane Complex of Zinc(II). *Inorg. Chem.* **1995**, *34*, 5606-5614. https://doi.org/10.1021/ic00126a034
- 26. Koziol, L.; Valdez, C. A.; Baker, S. E.; Lau, E. Y.; Floyd, W. C., III; Wong, S. E.; Satcher, J. H., Jr.; Lightstone, F. C.; Aines, R. D., Toward a Small Molecule, Biomimetic Carbonic Anhydrase Model: Theoretical and Experimental Investigations of a Panel of Zinc(II) Aza-Macrocyclic Catalysts. *Inorg. Chem.* **2012**, *51*, 6803-6812. https://doi.org/10.1021/ic300526b
- 27. Floyd, W. C., 3rd; Baker, S. E.; Valdez, C. A.; Stolaroff, J. K.; Bearinger, J. P.; Satcher, J. H., Jr.; Aines, R. D., Evaluation of a Carbonic Anhydrase Mimic for Industrial Carbon Capture. *Environ. Sci. Technol.* **2013**, *47*, 10049-55. https://doi.org/10.1021/es401336f
- 28. Yong, J. K. J.; Stevens, G. W.; Caruso, F.; Kentish, S. E., The Use of Carbonic Anhydrase to Accelerate Carbon Dioxide Capture Processes. *J. Chem. Technol. Biotechnol.* **2015**, *90*, 3-10. https://doi.org/10.1002/jctb.4502
- 29. Jin, C.; Zhang, S.; Zhang, Z.; Chen, Y., Mimic Carbonic Anhydrase Using Metal–Organic Frameworks for CO₂ Capture and Conversion. *Inorg. Chem.* **2018**, *57*, 2169-2174. https://doi.org/10.1021/acs.inorgchem.7b03021

- 30. Park, D.; Lee, M. S., Kinetic Study of CO₂ Hydration by Small-Molecule Catalysts with A Second Coordination Sphere that Mimic the Effect of the Thr-199 Residue of Carbonic Anhydrase. *Biomimetics* **2019**, *4*. https://doi.org/10.3390/biomimetics4040066
- 31. Woolley, P., Models for Metal Ion Function in Carbonic Anhydrase. *Nature (London, U. K.)* **1975**, *258*, 677-682. https://doi.org/10.1038/258677a0
- 32. Zhang, X.; van Eldik, R.; Koike, T.; Kimura, E., Kinetics and Mechanism of the Hydration of Carbon Dioxide and Dehydration of Bicarbonate Catalyzed by a Zinc(II) Complex of 1,5,9-Triazacyclododecane as a Model for Carbonic Anhydrase. *Inorg. Chem.* **1993**, *32*, 5749-5755. https://doi.org/10.1021/ic00077a017
- 33. Behnood, A.; Van Tittelboom, K.; De Belie, N., Methods for Measuring pH in Concrete: A Review. *Constr. Build. Mater.* **2016**, *105*, 176-188. https://doi.org/10.1016/j.conbuildmat.2015.12.032
- 34. Goñi, S.; Andrade, C., Synthetic Concrete Pore Solution Chemistry and Rebar Corrosion Rate in the Presence of Chlorides. *Cem. Concr. Res.* **1990**, *20*, 525-539. https://doi.org/https://doi.org/10.1016/0008-8846(90)90097-H
- 35. Vargová, Z.; Kotek, J.; Rudovský, J.; Plutnar, J.; Gyepes, R.; Hermann, P.; Györyová, K.; Lukeš, I., Ternary Complexes of Zinc(II), Cyclen and Pyridinecarboxylic Acids. *Eur. J. Inorg. Chem.* **2007**, *2007*, 3974-3987. https://doi.org/10.1002/ejic.200700183
- 36. Gudiksen, K. L.; Gitlin, I.; Moustakas, D. T.; Whitesides, G. M., Increasing the Net Charge and Decreasing the Hydrophobicity of Bovine Carbonic Anhydrase Decreases the Rate of Denaturation with Sodium Dodecyl Sulfate. *Biophys. J.* **2006**, *91*, 298-310. https://doi.org/10.1529/biophysj.106.081547
- 37. Hansen, J. H.; Petersen, S. V.; Andersen, K. K.; Enghild, J. J.; Damhus, T.; Otzen, D., Stable Intermediates Determine Proteins' Primary Unfolding Sites in the Presence of Surfactants. *Biopolymers* **2009**, *91*, 221-231. https://doi.org/10.1002/bip.21125
- 38. Jafari, M.; Mehrnejad, F.; Rahimi, F.; Asghari, S. M., The Molecular Basis of the Sodium Dodecyl Sulfate Effect on Human Ubiquitin Structure: A Molecular Dynamics Simulation Study. *Sci Rep* **2018**, *8*, 2150. https://doi.org/10.1038/s41598-018-20669-7

- 39. Li, J.; Fan, T.; Xu, Y.; Wu, X., Ionic Liquids as Modulators of Physicochemical Properties and Nanostructures of Sodium Dodecyl Sulfate in Aqueous Solutions and Potential Application in Pesticide Microemulsions. *Phys. Chem. Chem. Phys.* **2016**, *18*, 29797-29807. https://doi.org/10.1039/C6CP04722J
- 40. Jeppsson, L.; Anehus, R., A Buffered Formic Acid Technique for Conodont Extraction. *J. Paleontol.* **1995**, *69*, 790-794. https://doi.org/10.1017/S0022336000035319
- 41. Anderegg, G.; Hubmann, E.; Podder, N. G.; Wenk, F., Pyridinderivate als Komplexbildner. XI. Die Thermodynamik der Metallkomplexbildung mit Bis-, Trisund Tetrakis[(2-pyridyl)methyl]-aminen. *Helv. Chim. Acta* **1977**, *60*, 123-140. https://doi.org/10.1002/hlca.19770600115
- 42. Al-Hosney, H. A.; Carlos-Cuellar, S.; Baltrusaitis, J.; Grassian, V. H., Heterogeneous Uptake and Reactivity of Formic Acid on Calcium Carbonate Particles: A Knudsen Cell Reactor, FTIR and SEM Study. *Phys. Chem. Chem. Phys.* **2005**, *7*, 3587-3595. https://doi.org/10.1039/B510112C
- 43. Lv, B.; Guo, B.; Zhou, Z.; Jing, G., Mechanisms of CO₂ Capture into Monoethanolamine Solution with Different CO₂ Loading during the Absorption/Desorption Processes. *Environ. Sci. Technol.* **2015**, *49*, 10728-10735. https://doi.org/10.1021/acs.est.5b02356
- 44. Nakagaki, T.; Tanaka, I.; Furukawa, Y.; Sato, H.; Yamanaka, Y., Experimental Evaluation of Effect of Oxidative Degradation of Aqueous Monoethanolamine on Heat of CO₂ Absorption, Vapor Liquid Equilibrium and CO₂ Absorption Rate. *Energy Procedia* **2014**, *63*, 2384-2393. https://doi.org/10.1016/j.egypro.2014.11.260
- 45. Gitlin, I.; Gudiksen, K. L.; Whitesides, G. M., Peracetylated Bovine Carbonic Anhydrase (BCA-Ac18) Is Kinetically More Stable than Native BCA to Sodium Dodecyl Sulfate. *J. Phys. Chem. B* **2006**, *110*, 2372-2377. https://doi.org/10.1021/jp055699f
- 46. da Silva, E. F.; Svendsen, H. F., Ab Initio Study of the Reaction of Carbamate Formation from CO₂ and Alkanolamines. *Ind. Eng. Chem. Res.* **2004**, *43*, 3413-3418. https://doi.org/10.1021/ie030619k
- 47. de Ávila, S. G.; Logli, M. A.; Silva, L. C. C.; Fantini, M. C. A.; Matos, J. R., Incorporation of Monoethanolamine (MEA), Diethanolamine (DEA) and Methyldiethanolamine (MDEA) in Mesoporous Silica: An Alternative to CO₂ Capture. *J. Environ. Chem. Eng.* **2016**, *4*, 4514-4524. https://doi.org/10.1016/j.jece.2016.10.015

- 48. Han, B.; Zhou, C.; Wu, J.; Tempel, D. J.; Cheng, H., Understanding CO₂ Capture Mechanisms in Aqueous Monoethanolamine via First Principles Simulations. *J. Phys. Chem. Lett.* **2011**, *2*, 522-526. https://doi.org/10.1021/jz200037s
- 49. Li, K.; Cousins, A.; Yu, H.; Feron, P.; Tade, M.; Luo, W.; Chen, J., Systematic Study of Aqueous Monoethanolamine-based CO₂ Capture Process: Model Development and Process Improvement. *Energy Sci. Eng.* **2016**, *4*, 23-39. https://doi.org/10.1002/ese3.101
- 50. McCann, N.; Phan, D.; Wang, X.; Conway, W.; Burns, R.; Attalla, M.; Puxty, G.; Maeder, M., Kinetics and Mechanism of Carbamate Formation from CO_{2(aq)}, Carbonate Species, and Monoethanolamine in Aqueous Solution. *J. Phys. Chem. A* **2009**, *113*, 5022-5029. https://doi.org/10.1021/jp810564z
- 51. Puxty, G.; Rowland, R.; Allport, A.; Yang, Q.; Bown, M.; Burns, R.; Maeder, M.; Attalla, M., Carbon Dioxide Postcombustion Capture: A Novel Screening Study of the Carbon Dioxide Absorption Performance of 76 Amines. *Environ. Sci. Technol.* **2009**, *43*, 6427-6433. https://doi.org/10.1021/es901376a
- 52. Widger, L. R.; Sarma, M.; Kelsey, R. A.; Risko, C.; Lippert, C. A.; Parkin, S. R.; Liu, K., Enhancing CO₂ absorption for post-combustion carbon capture via zinc-based biomimetic catalysts in industrially relevant amine solutions. *Int. J. Greenhouse Gas Control* **2019**, *85*, 156-165. https://doi.org/10.1016/j.ijggc.2019.04.002

9. Table of Contents Only

